PLOS COMPUTATIONAL BIOLOGY

RESEARCH ARTICLE

Computational study on ratio-sensing in yeast galactose utilization pathway

Jiayin Hong[1], **Bo Hua**[2], **Michael Springer**[2]*, **Chao Tang**[1,3]*

1 Center for Quantitative Biology and Peking-Tsinghua Center for Life Sciences, Academy for Advanced Interdisciplinary Studies, Peking University, Beijing, China, **2** Department of Systems Biology, Harvard Medical School, Boston, Massachusetts, United States of America, **3** School of Physics, Peking University, Beijing, China

* michael_springer@hms.harvard.edu (MS); tangc@pku.edu.cn (CT)

OPEN ACCESS

Citation: Hong J, Hua B, Springer M, Tang C (2020) Computational study on ratio-sensing in yeast galactose utilization pathway. PLoS Comput Biol 16(12): e1007960. https://doi.org/10.1371/journal.pcbi.1007960

Editor: Pedro Mendes, University of Connecticut School of Medicine, UNITED STATES

Received: May 13, 2020

Accepted: October 16, 2020

Published: December 4, 2020

Data Availability Statement: All relevant data are within the manuscript and its Supporting Information files.

Funding: JH and CT were supported by National Natural Science Foundation of China (91430217). JH was supported by China Scholarship Council for one-year study at Harvard University. MS is supported by National Institutes of Health under grant no. R01-GM120122-03. The funders had no role in study design, data collection and analysis, decision to publish, or preparation of the manuscript.

Abstract

Metabolic networks undergo gene expression regulation in response to external nutrient signals. In microbes, the synthesis of enzymes that are used to transport and catabolize less preferred carbon sources is repressed in the presence of a preferred carbon source. For most microbes, glucose is a preferred carbon source, and it has long been believed that as long as glucose is present in the environment, the expression of genes related to the metabolism of alternative carbon sources is shut down, due to catabolite repression. However, recent studies have shown that the induction of the galactose (GAL) metabolic network does not solely depend on the exhaustion of glucose. Instead, the GAL genes respond to the external concentration ratio of galactose to glucose, a phenomenon of unknown mechanism that we termed ratio-sensing. Using mathematical modeling, we found that ratio-sensing is a general phenomenon that can arise from competition between two carbon sources for shared transporters, between transcription factors for binding to communal regulatory sequences of the target genes, or a combination of the aforementioned two levels of competition. We analyzed how the parameters describing the competitive interaction influenced ratio-sensing behaviors in each scenario and found that the concatenation of both layers of signal integration could expand the dynamical range of ratio-sensing. Finally, we investigated the influence of circuit topology on ratio-sensing and found that incorporating negative auto-regulation and/or coherent feedforward loop motifs to the basic signal integration unit could tune the sensitivity of the response to the external nutrient signals. Our study not only deepened our understanding of how ratio-sensing is achieved in yeast GAL metabolic regulation, but also elucidated design principles for ratio-sensing signal processing that can be used in other biological settings, such as being introduced into circuit designs for synthetic biology applications.

Author summary

Microbes make sophisticated choices about the uptake and metabolism of nutrients depending on the variety of nutrient choices available to them in their environment. In

Competing interests: The authors have declared that no competing interests exist.

the well-studied yeast galactose utilization network, a recent study has shown that galactose metabolic genes respond to the external concentration ratio of galactose to glucose. Using computational models, we showed that this type of phenomenon could arise from a competition between galactose and glucose for transporters, a competition between transcription factors for promoters, or a combination of these two mechanisms. We further revealed the controlling parameters that determined the system sensitivity towards competing input signals and that determined the concentration ratio required to induce the metabolic network in each scenario. Combining competition inhibition at both the transporter level and the transcriptional level can enlarge the ratio-sensing regime, resulting a robust signal integration module. We suspect that modules of this kind may be common in many areas of biology.

Introduction

Carbon catabolite repression (CCR) is a conserved phenomenon in microorganisms[1–6]. In 1942, Jacques Monod found that when cultured in two carbon sources, bacteria exhibit diauxic growth[7], i.e. they consume the preferred carbon source until it is exhausted, then switch to the less preferred source. This phenomenon was later also observed in yeast[8], for example in the galactose utilization pathway (GAL), which is activated when glucose in the culture is exhausted[9–11]. A recent study has shown that the induction of the GAL pathway in yeast cells is determined not by the absolute level of glucose, but by the concentration ratio of external galactose to external glucose[12]. This mode of induction is termed ratio-sensing. Another study has shown that ratio-sensing is closely related to optimal allocation of protein resources within a cell[13]. A similar ratiometric response, functioning to integrate competing signals, has been identified in the mammalian Bone Morphogenetic Protein (BMP) signaling pathway [14]. Since ratio-sensing responses may have broad importance in biology, we set out to determine what types of general mechanisms can lead to a ratio-sensing response. We constructed simplified mathematical models of competitive binding at both the transporter and transcriptional levels for a simplified version of the GAL pathway in yeast (diagrammed in Fig 1A), and found that either could be responsible for a ratio-metric response.

To quantitatively determine how glucose depresses GAL pathway induction, we defined a parameter, the "decision condition" that described the nutrient conditions in which the yeast cells showed half maximum induction of the GAL network. When the decision conditions were plotted on a log-log scale plot of glucose versus galactose concentrations, the curve described by these points was termed the decision front (Fig 1B). The slope of the decision front represents the relative sensitivity of the signal integration unit to the competing input signals. When the decision front undergoes a parallel shift, this indicates a change of the concentration ratio that is required to induce the GAL network.

Sugar uptake in yeast is mediated by a variety of transporters. The hexose transporter family (HXT) consists of 17 members, HXT1-HXT17, with varied binding affinity to glucose and other hexoses[15–18]. Gal2p is a galactose permease located in the cellular membrane, which has comparable binding affinity for both galactose and glucose[19]. This suggests that competition at the transporter level between glucose and galactose is possible. Another possible mechanism involves Gal3p, the internal sensor of galactose (see Fig 1A). When Gal3p binds to galactose it relieves the sequestration of Gal4p by Gal80p, causing transcriptional activation of the downstream GAL metabolic genes including GAL1, GAL2, GAL3, and GAL80[20–26]. If glucose is also present, the internal sensor of glucose, Mig1, transcriptionally represses GAL

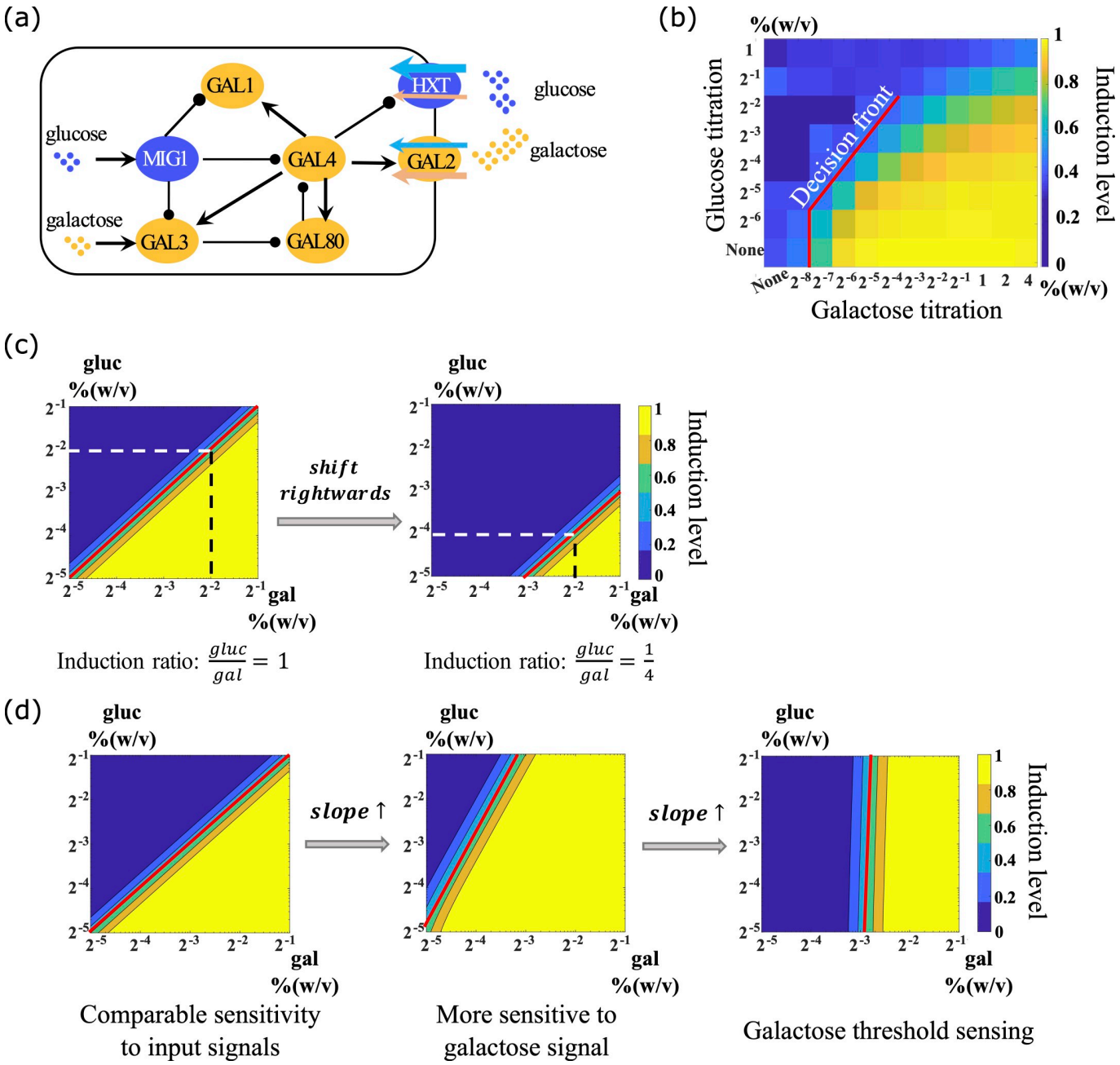

Fig 1. Ratiometric response and the decision front to induce the GAL network. (a) The galactose metabolic gene regulatory network in yeast. (b) Galactose metabolic genes respond to the ratio of external concentrations of galactose and glucose. Different combinations of nutrient concentrations were given to the yeast as indicated by the x and y axes (extracellular sugar concentrations). The color indicates the induction level of the GAL network in each combination of the concentrations. The decision front was defined as the contour line of a fixed induction level. (Data from Ref. [12]). (c) The intercept on the galactose titration axis indicates the induction ratio of glucose to galactose that was required to induce the GAL network. A parallel shift towards higher galactose concentration represents strains that are more susceptible to glucose repression. (d) The slope of the decision front reflects the network relative sensitivity to each nutrient. The contour lines represent specific induction levels of the GAL network. Increasing the slope of the decision front corresponds to elevated sensitivity to the activating galactose signal, and a vertical decision front corresponds to galactose threshold sensing.

https://doi.org/10.1371/journal.pcbi.1007960.g001

metabolic genes including GAL1, GAL3 and GAL4[27–30]. In other words, intracellular glucose represses the induction of the GAL pathway through transcriptional inhibition by activating Mig1, indicating that competitive inhibition may also operate at the transcriptional level.

As shown in the diagram (Fig 1A), there are thus two ways that galactose can be prevented from activating the GAL pathway: high levels of glucose can prevent galactose from entering the cell through competitive binding to the communal transporters HXT and Gal2p, and/or the activation of Mig1 can interfere with transcriptional activation of the pathway by Gal4p. We set out to determine which of these mechanisms can explain the ratio-sensing behavior that was observed experimentally. Due to the complexity of the glucose network and insufficient information on the parameter values, we followed similar simplifications of the model that were implemented by Bennett et. al. [31], in which they used a heuristic set of equations to describe a basic transport regulatory system. Specifically, in the transporter model, hexose transporters are responsible for transporting external glucose and galactose into the cell, whereas in the transcriptional regulatory model, internalized glucose acts to induce transcriptional inhibition in the galactose network through the binding of the repressor to the cis-regulatory elements of GAL1 (akin to Mig1 activity). We found that each of these mechanisms could produce ratio-sensing behavior, and combining both mechanisms produced a robust signal integration mechanism that delivered ratio-sensing behavior over a wide range of input parameters.

Results

Decision front

The induction of the galactose metabolic genes in yeast is controlled by both the concentration of galactose and the concentration of glucose in the environment. All lab yeasts and natural yeast isolates studied so far show a ratio-sensing response, but the nutrient conditions required to induce the GAL network vary from one strain to another[12]. Yeast cells were cultured in different combinations of glucose and galactose, and each tile in Fig 1B represent one of the nutrient conditions. As glucose inhibits the induction of the GAL pathway whereas galactose promotes it, yeast cells cultured in different nutrient conditions showed varied induction levels. The promoter of GAL1 was fused with yellow fluorescence proteins and the fluorescent intensity was measured to indicate the induction levels [12]. All of the induction levels in a range of nutrient conditions were normalized to the maximum induction level, which in theory is the induction level at highest galactose and lowest glucose concentrations (the lower right corner). The color codes for normalized induction levels. To quantitatively study signal integration in the GAL network, we built coarse-grained ODE models (see Methods and Models, and S1 Text for details) that described the reactions that occur at the transporter level and the transcriptional level, and simulated the behavior of the network when induced by double gradients of glucose and galactose (Fig 1C and 1D). The contour lines in the double titration graph delineate specific induction levels of the GAL network. Each point on a contour line represents a combination of glucose and galactose concentrations that results in the same induction level of the GAL pathway. We call this contour line the decision front. To better understand the possible types of behaviors from our model, we will describe what several different types of qualitative changes would mean in terms of glucose and galactose regulation. This explanation will help to understand the behaviors observed throughout the paper.

Each yeast isolate has a characteristic decision front, representing the concentration ratio required to induce the GAL network in that strain (Fig 1C). As the decision front shifts rightwards along the galactose titration axis, the induction ratio of glucose to galactose decreases from 1 to ¼, indicating that the strains require more galactose to be present in their environment before they induce the GAL network.

The slope of the decision front reflects how sensitive the yeast strain is to the presence of galactose and glucose (Fig 1D). An increased slope of the decision front reflects greater

sensitivity to the activating galactose signal than to the suppressing glucose signal. Strains with decision front almost vertical to the galactose titration axis indicate that induction of the GAL pathway is almost independent of external glucose in these strains. In contrast, a decreased slope of the decision front indicates increased sensitivity to suppression by glucose.

Realizing ratio-sensing by competitive binding to the communal transporter

How is ratio-sensing implemented at the molecular level? We first focused on the possibility that transporter competition was responsible. We abstracted the uptake of glucose and galactose through HXT and Gal2p as a simplified mathematical model (see Methods and Models for model derivations, and S1 Table for parameter descriptions and units). Galactose and glucose are transported into the cell by a shared transporter, with binding coefficients of K_{gal} and K_{gluc}, and cooperativity coefficients of n_{gal} and n_{gluc}, respectively (Fig 2A). We assumed that the total number of transporters within a cell was constant and had three states: bound by glucose, bound by galactose, or empty. We simulated transport of both sugars under these conditions (Fig 2B and 2C, the parameter values used in these simulations can be found in S2 Table), and assumed that the GAL network would be induced when the intracellular galactose level was above a threshold concentration of galactose. Solving the equations that describe the dynamics of intracellular galactose and glucose, and that of different states of membrane transporters (see Methods and Models, Eqs 11–15) at steady state yielded an expression describing the intracellular galactose level in terms of external glucose and galactose.

$$gal_{in} = \frac{k_{trans}}{\gamma} \cdot T_{total} \cdot \frac{1}{1 + \frac{K_{gal}}{gal_{ex}} \cdot \left(1 + \frac{gluc_{ex}}{K_{gluc}}\right)} \tag{1}$$

In Eq (1), k_{trans} is the maximal transportation rate through the given transporter, γ is the turn-over rate of the sugar within a cell, T_{total} is the total number of transporters expressed on the membrane, K_{gal} and K_{gluc} are the binding coefficients for galactose and glucose respectively, and gal_{ex} and $gluc_{ex}$ are the concentrations of the external carbon sources. Eq (1) suggests that when the maximal transportation rate and turn-over rate within a cell are fixed, a ratio-sensing regime exists as long as the binding affinity coefficient between glucose and the transporter is much smaller than the external glucose concentration ($K_{gluc} \ll gluc_{ex}$), i.e. the external glucose level is high enough to saturate the transporters.

Next, we derived the expression of the decision front in log-log scale as follows:

$$log\ gluc_{ex} = \frac{n_{gal}}{n_{gluc}} \cdot log\ gal_{ex} + \frac{1}{n_{gluc}} \cdot log \frac{{K_{gluc}}^{n_{gluc}}}{{K_{gal}}^{n_{gal}}} + const \tag{2}$$

where n_{gal} and n_{gluc} are the cooperativity coefficients of galactose and glucose binding to the transporter, respectively. From Eq (2) we know that the intercept on the galactose titration axis is determined by the relative binding affinity between the two sugars and the communal transporters. This explains why the decision front shifted to a higher $\frac{gal}{gluc}$ ratio as we increased $\frac{K_{gal}}{K_{gluc}}$ (Fig 2B). This makes intuitive sense: the stronger the binding between glucose and the transporter, or the weaker the binding between galactose and the transporter, the more the GAL network should be inhibited by glucose and the higher the level of external galactose required to induce the GAL pathway.

Note that when the condition $K_{gluc} \ll gluc_{ex}$ is met, we observe a ratio regime across the full physiological plausible range of double sugar titration. In contrast, when $K_{gluc} \ll gluc_{ex}$ is violated, the system exhibits a compound signal integration mode, i.e. at low concentrations of

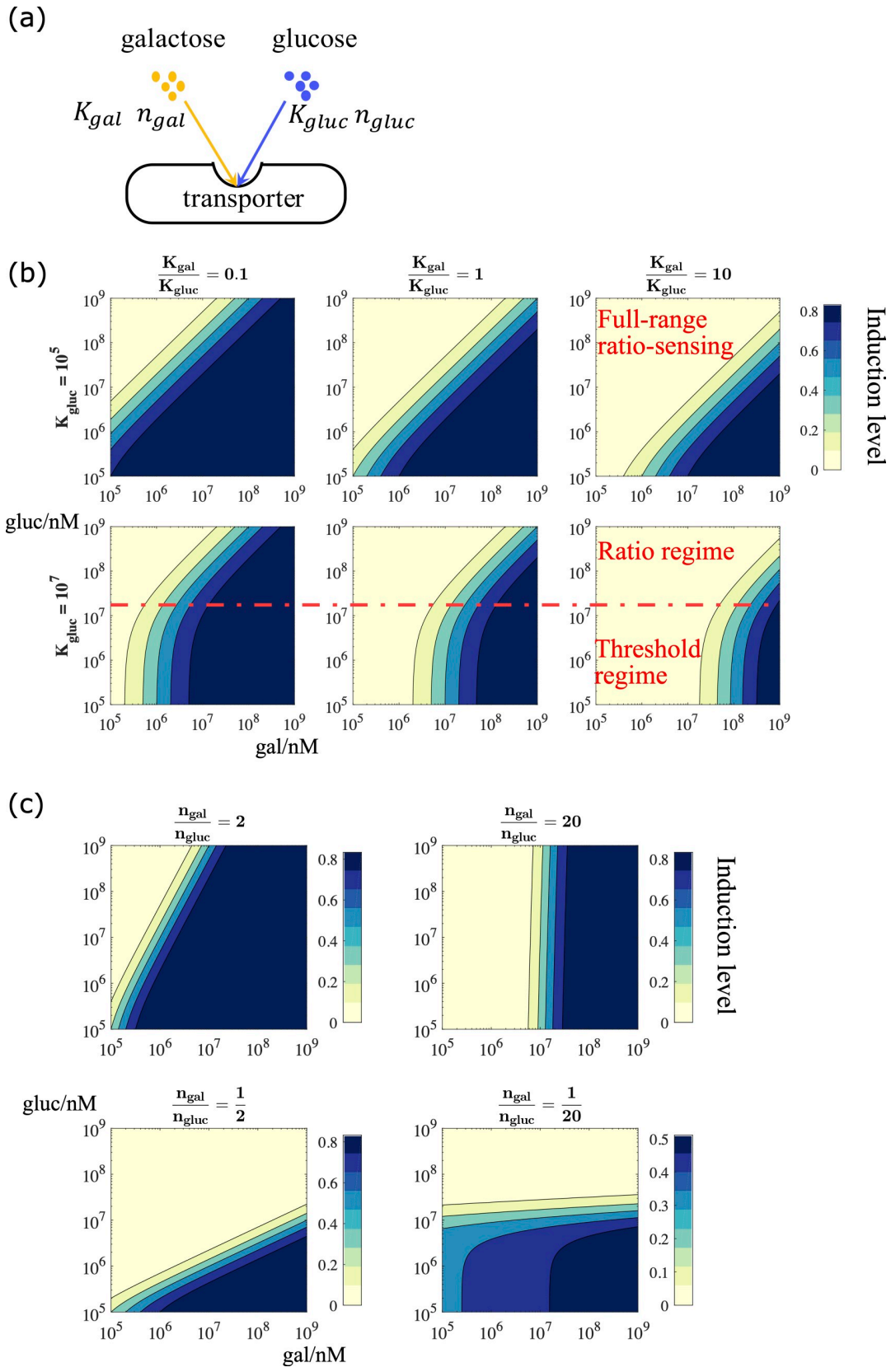
(a)
galactose
glucose
K_{gal} n_{gal}
K_{gluc} n_{gluc}
transporter
(b)
$\frac{K_{gal}}{K_{gluc}} = 0.1$
$\frac{K_{gal}}{K_{gluc}} = 1$
$\frac{K_{gal}}{K_{gluc}} = 10$
$K_{gluc} = 10^5$
$K_{gluc} = 10^7$
Full-range ratio-sensing
Ratio regime
Threshold regime
gluc/nM
gal/nM
Induction level
(c)
$\frac{n_{gal}}{n_{gluc}} = 2$
$\frac{n_{gal}}{n_{gluc}} = 20$
$\frac{n_{gal}}{n_{gluc}} = \frac{1}{2}$
$\frac{n_{gal}}{n_{gluc}} = \frac{1}{20}$
gluc/nM
gal/nM
Induction level

Fig 2. Realizing ratio-sensing by competitive binding to the communal transporter. (a) The transporter level competitive binding model. (b) Simulations of the induction level of the GAL pathway in the transporter level model. While keeping K_{gluc} unchanged, increasing the relative binding affinity $\frac{K_{gal}}{K_{gluc}}$ shifts the decision front towards higher galactose concentration. The upper panel parameter regime with $K_{gluc} = 10^5$ exhibits a full-range ratiometric response, whereas the lower panel parameter regime with $K_{gluc} = 10^7$ exhibits a compound signal integration mode, i.e. galactose threshold sensing at poor nutrient condition and ratio-sensing at rich nutrient condition. (c) The network sensitivity to input signals is determined by relative binding cooperativity. Increasing the relative cooperativity makes the signal integration unit more sensitive to activating galactose signal, whereas decreasing the relative cooperativity makes the signal integration unit more sensitive to repressing glucose signal. In the extreme case, where the decision front is almost vertical to the galactose titration axis $\left(\frac{n_{gal}}{n_{gluc}} = 20\right)$, the signal integration unit becomes a galactose threshold sensor. When the decision front is almost parallel to the galactose titration axis $\left(\frac{n_{gal}}{n_{gluc}} = \frac{1}{20}\right)$, the signal integration unit becomes a glucose threshold sensor. (b)-(c) Parameter values used in these simulations can be found in S2 Table.

https://doi.org/10.1371/journal.pcbi.1007960.g002

both glucose and galactose, the GAL pathway responds solely to the external galactose signal. In other words, we observe a galactose threshold sensing at low concentrations of sugars, but at high concentrations of both sugars we see a ratio-sensing response. This is consistent with the experimental observations reported by Escalante-Chong et al[12]. The analytical derivation also shows that the slope of the decision front is determined by the relative cooperativity of galactose and glucose binding to the transporter. Varying the value of $\frac{n_{gal}}{n_{gluc}}$ changed the slope of the decision front, and when $\frac{n_{gal}}{n_{gluc}} > 1$, the system is more sensitive to the external galactose signal. With $\frac{n_{gal}}{n_{gluc}} = 20$, the system becomes almost independent of glucose concentrations, i.e. galactose threshold sensing, for a portion of the phase space as seen in Fig 2C. In contrast, when $\frac{n_{gal}}{n_{gluc}} < 1$, the system is more sensitive to the external glucose signal. With $\frac{n_{gal}}{n_{gluc}} = \frac{1}{20}$, the system becomes almost solely responsive to the variation of glucose concentration, i.e. glucose threshold sensing (Fig 2C).

Realizing ratio-sensing by transcriptional inhibition of GAL metabolic genes

Apart from the cross-talk at the transporter level, glucose also inhibits the expression of GAL genes through the activation of the transcription factor Mig1. We generalized this mechanism as a two-step reaction, and explored whether it can also produce a ratio-sensing response (Fig 3A). In the first step of this reaction system, both the activating signal (galactose) and the inhibiting signal (glucose) bind to their corresponding intracellular sensors, forming the activator (Gal3p*) and the repressor (Mig1*). In the second step, either the activator or the repressor binds to a cis-regulatory element (CRE) of the readout (GAL1), where the conflicting effect was integrated at the transcriptional level. Again, we used the law of mass action to model the association and dissociation between the sugars and the sensors, and that between the sensors and the CRE (see Methods and Models for model derivations, and S1 Table for parameter descriptions and units). Here, we assumed that the copy number of the GAL1 gene was constant within a cell, and the CRE of GAL1 had three possible states: bound by the activator and transcriptionally active; bound by the repressor and thus transcriptionally inhibited; and free such that it is not inhibited but not transcribing. Because the biochemical reactions of binding and unbinding between sugars and sensors are much more rapid than the process of transcription[32], we used separation of time-scale in our model and obtained a quasi-equilibrium approximation for the functional forms of the activator and the repressor:

$$Activator^* = \frac{gal_{in}}{K_G + gal_{in}} \cdot Activator_{total} \tag{3}$$

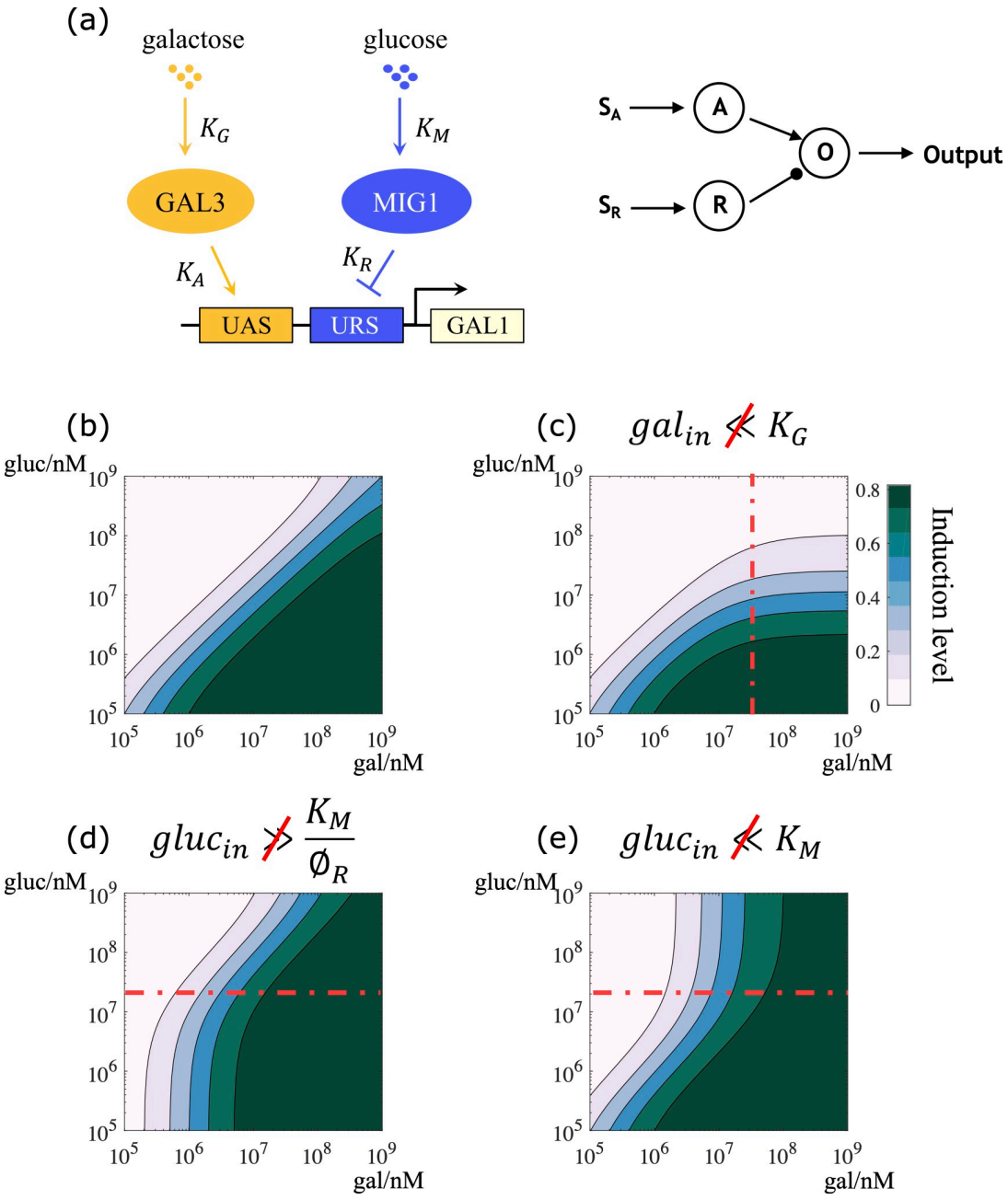

Fig 3. Realizing ratio-sensing by transcriptional inhibition of GAL metabolic genes. (a) The transcriptional level competitive inhibition model. An abstract transcriptional circuit of the GAL pathway is shown on the left, and the generalized transcriptional circuit is shown on the right. Galactose and glucose correspond to activating signal S_A and repressing signal S_R, respectively. Gal3p and Mig1 correspond to the activator and the repressor, respectively. The expression level of GAL1 is the output of the circuit. (b) The transcriptional level model can give rise to a full-range ratiometric response in a reasonable parameter regime. (c) When the requirement $gal_{in} \ll K_G$ is violated, the signal integration unit exhibits ratio-sensing at low carbon source concentrations, and glucose threshold sensing at high carbon source concentrations. (d) When the requirement $gluc_{in} \gg \frac{K_M}{\emptyset_R}$ is violated, the signal integration unit exhibits galactose threshold sensing at low carbon source concentrations, and ratio-sensing at high carbon source concentrations. (e) When the requirement $gluc_{in} \ll K_M$ is violated, the signal integration unit exhibits ratio-sensing at low carbon source concentrations, and galactose threshold sensing at high carbon source concentrations. (b)-(e) Parameter values used in these simulations can be found in S3 Table.

https://doi.org/10.1371/journal.pcbi.1007960.g003

$$Repressor^{*} = \frac{gluc_{in}}{K_M + gluc_{in}} \cdot Repressor_{total} \quad (4)$$

where $K_G = \frac{kr_G}{kf_G}$, and $K_M = \frac{kr_M}{kf_M}$, denoting the binding affinity of galactose and glucose to their corresponding intracellular sensors, respectively, and $Activator_{total}$ and $Repressor_{total}$ are the total amount (free forms plus functional forms) of the activator and the repressor.

When the association and dissociation between the cis- and trans-regulatory elements of GAL1 reaches equilibrium, the fraction of actively-transcribed genes among the total number of GAL1 copies is:

$$\frac{\mathrm{GAL1}_{\mathrm{active}}}{\mathrm{GAL1}_{\mathrm{total}}} = \frac{1}{1 + \frac{1}{\emptyset_A} \cdot \left(\frac{K_G}{gal_{in}} + 1\right) \cdot \left(1 + \frac{\emptyset_R}{\frac{K_M}{gluc_{in}} + 1}\right)} \quad (5)$$

where $\emptyset_A = \frac{Activator_{total}}{K_A}$, and $\emptyset_R = \frac{Repressor_{total}}{K_R}$. K_A and K_R are the dissociation constants of the activator and the repressor binding to the CRE of GAL1, respectively. Analytical derivation showed that a ratio-sensing regime emerged when the following requirements were simultaneously met: $gal_{in} \ll K_G$ and $\frac{K_M}{\emptyset_R} \ll gluc_{in} \ll K_M$. The decision front is described by:

$$log\ gluc_{in} = log\ gal_{in} + log\frac{K_M}{K_G} + log\frac{\emptyset_A}{\emptyset_R} + const \quad (6)$$

Eq (6) indicates that the slope of the decision front in a basic signal integration circuit is fixed at 1, and the intercept on the galactose titration axis is determined by $\frac{K_G}{K_M} \times \frac{\emptyset_R}{\emptyset_A}$, where K_G and K_M represent the binding affinity of galactose to the activator, and of glucose to the repressor, respectively. $\emptyset_R$ measures the repression capacity of the repressor, with greater values signaling stronger inhibition. Similarly, $\emptyset_A$ represents the activation capacity of the activator.

Numerical simulations of this system (parameter values used in these simulations can be found in S3 Table) shows that ratio-sensing is achieved if $gal_{in} \ll K_G$ and $\frac{K_M}{\emptyset_R} \ll gluc_{in} \ll K_M$ are simultaneously met (Fig 3B). Violation of any of these requirements results in a combination of ratio-sensing and threshold sensing. Specifically, when $gal_{in} \ll K_G$ is violated, the system responds to the ratio of the two nutrient signals at low input concentrations, but only responds to changes in glucose levels at high input concentrations (Fig 3C). When $gluc_{in} \gg \frac{K_M}{\emptyset_R}$ is violated, the system exhibits galactose threshold sensing at low input concentrations, but responds to the concentration ratio at high input concentrations (Fig 3D). Lastly, when $gluc_{in} \ll K_M$ is violated, the system exhibits ratio-sensing at low input concentrations, but responds only to changes in galactose levels at high input concentrations (Fig 3E).

A combination of both transporter-level and transcription-level competition expands the dynamical range of ratio-sensing

Our analysis showed that ratio-sensing could arise from either competitive binding to the shared transporters alone, or from transcriptional regulation of the GAL metabolic genes alone. Since glucose and galactose do compete for Gal2p and HXTs, and transcriptional inhibition of the GAL metabolic genes by Mig1 also occurs, we were curious about whether there is a benefit to yeast cells that could use both mechanisms for ratiometric signal integration. We therefore modeled a combination of both mechanisms, using the output of the competitive

transporter model as the input of the transcriptional regulation model, to investigate how the combined system behaved.

We combined two typical signal integration behaviors from the transporter model (Fig 4A) with four typical signal integration behaviors of transcriptional model (Fig 4B), and simulated the response of the resultant eight combinations (Fig 4C, parameter values used in the

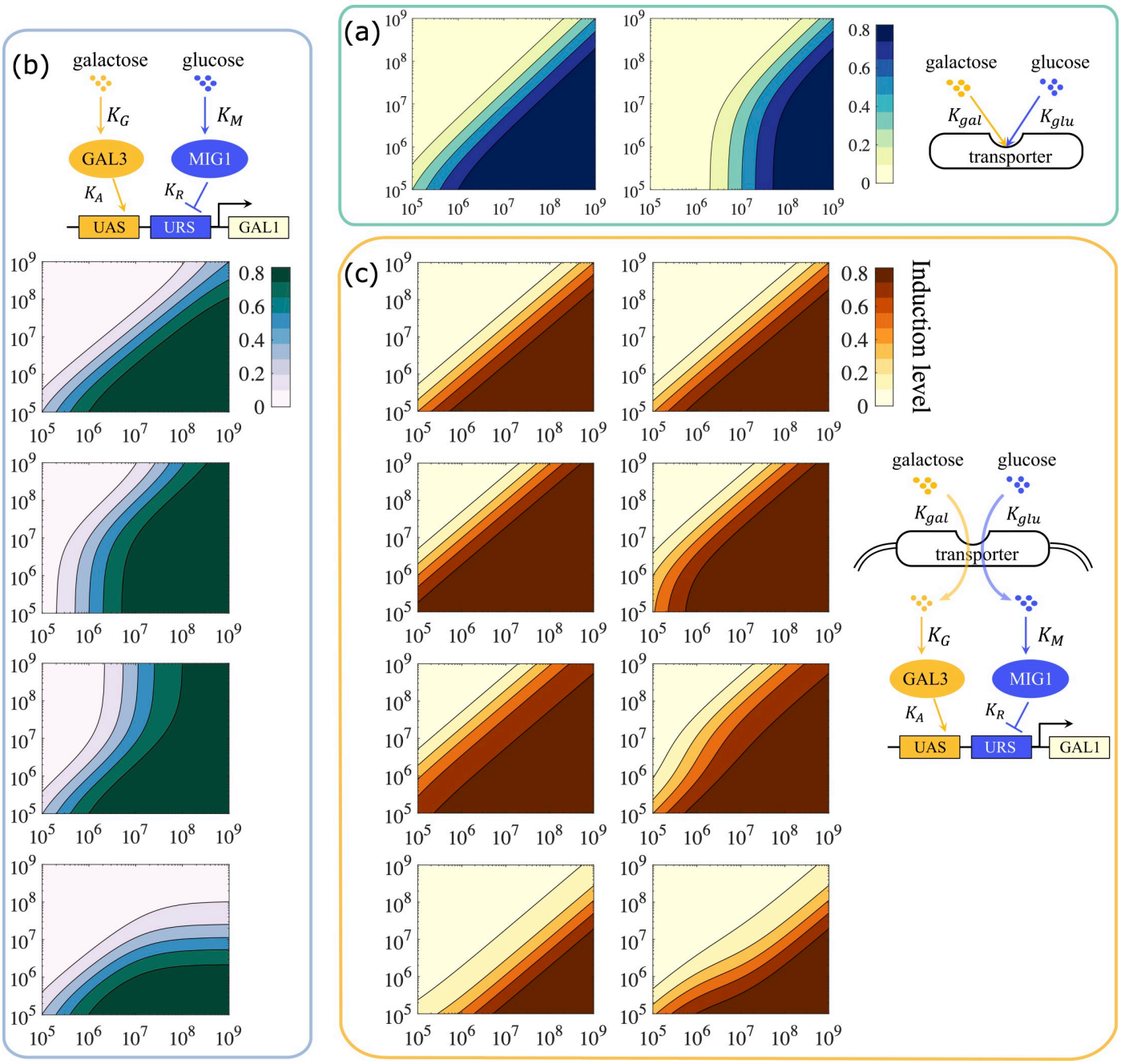

Fig 4. Concatenating the dual layers of signal integration expanded the dynamical range of ratio-sensing. (a) The two typical signal response patterns in the transporter level model. The pattern on the left exhibits full-range ratio-sensing while the one on the right exhibits galactose threshold sensing combined with ratio-sensing. (b) The four typical signal response patterns in the transcriptional level model specified in Fig 3B–3E. (c) The output signal response patterns of the concatenation model all exhibit full-range ratio-sensing, despite the fact that some response patterns in either the upstream transporter layer or the downstream transcriptional layer showed compound signal integration. Parameter values used in the simulations can be found in S4 Table.

https://doi.org/10.1371/journal.pcbi.1007960.g004

simulations can be found in S4 Table). We found that, no matter whether the single integration modes were ratio-sensing or a mix of ratio-sensing and threshold sensing, all eight combinations exhibited ratio-sensing response. In other words, combining both mechanisms together expanded the dynamical range over which a ratiometric response was observed.

To determine the mechanism underlying this effect, we analyzed the requirements for ratio-sensing in the combined model. The transcriptional regulation model alone generates a ratiometric response only when $gal_{in} \ll K_G$ and $\frac{K_M}{\emptyset_R} \ll gluc_{in} \ll K_M$. In the combined model, both gal_{in} and $gluc_{in}$ are determined by the behavior of the hexose transporters. Hence, we used Eq (1) and

$$gluc_{in} = \frac{k_{trans}}{\gamma} \cdot T_{total} \cdot \frac{1}{1 + \frac{K_{gluc}}{gluc_{ex}} \cdot \left(1 + \frac{gal_{ex}}{K_{gal}}\right)} \tag{7}$$

to substitute gal_{in} and $gluc_{in}$, yielding the following requirements for ratio-sensing in the concatenation model:

$$\frac{1}{1 + \frac{K_{gal}}{gal_{ex}} \cdot \left(1 + \frac{gluc_{ex}}{K_{gluc}}\right)} \ll \frac{K_G}{\psi} \tag{8}$$

$$\frac{K_M}{\psi \cdot \emptyset_R} \ll \frac{1}{1 + \frac{K_{gluc}}{gluc_{ex}} \cdot \left(1 + \frac{gal_{ex}}{K_{gal}}\right)} \ll \frac{K_M}{\psi} \tag{9}$$

where $\psi = \frac{k_{trans} \cdot T_{total}}{\gamma}$ represents the sugar transportation capacity. Note that $\frac{1}{1 + \frac{K_{gal}}{gal_{ex}} \cdot \left(1 + \frac{gluc_{ex}}{K_{gluc}}\right)}$ and $\frac{1}{1 + \frac{K_{gluc}}{gluc_{ex}} \cdot \left(1 + \frac{gal_{ex}}{K_{gal}}\right)}$ are always smaller than 1, which means that as long as $K_G \gg \psi$ and $K_M \gg \psi$ are satisfied and $\emptyset_R$ is large, the system will respond in a ratiometric manner.

This analysis implies that when the external glucose concentration is low, causing the upstream transporter circuit to fall into a galactose threshold sensing pattern, the system is nevertheless able to realize ratio-sensing if the input sugars bind to their corresponding internal sensors with low affinity, so that $K_G \gg \psi$ and $K_M \gg \psi$ are satisfied. Conversely, when the adjustable capacity of the downstream transcriptional regulatory layer is limited, causing the CRE of GAL1 to be saturated by either the activator or the repressor, the system can realize ratio-sensing by reducing the production of transporters, so that $K_G \gg \psi$ and $K_M \gg \psi$ are again satisfied. Taken together, the combination of the two layers of molecular circuits increases the flexibility of signal integration, giving rise to an expanded ratio-sensing regime.

Incorporating network motifs to the basic signal integration unit altered the network sensitivity to input signals

In the model of competitive binding at the transporter level, we showed that the relative binding cooperativity of the competing sugars determined the sensitivity of the signal integration circuit to external nutrient signals, that is, the slope of the decision front can change as the system becomes more sensitive to one sugar than the other (Fig 2C). This stands in contrast to the transcription-level model, which always has a decision front with slope approximately equal to 1, i.e. the simple signal integration unit we modeled had comparable sensitivity to both of the competing input signals (Fig 3B). We were curious whether it is possible to alter the behavior of the system by changing the topology of the signal integration unit.

There are recurring regulatory patterns that appear in transcriptional networks much more frequently than would be expected for random networks. These patterns, called network motifs,

have been found in a range of organisms from microbes to mammalian cells[33–35]. We incorporated selected network motifs into our original model and tested how this changed the response to the nutrient stimuli (parameter values used in these simulations can be found in S5 Table). While the slope of the decision front in our original model was approximately 1 (Fig 5A), we found that introducing negative autoregulation[36,37] at the activator node, and/or introducing a negative regulatory edge from the repressor to the activator, forming a coherent feedforward loop [38], decreased the slope of the decision front, and made the signal integration unit more sensitive to the repressing nutrient signal (Fig 5B). In contrast, introducing negative autoregulation at the repressor node, and/or introducing a negative regulatory edge from the activator to the repressor, forming a coherent feedforward loop, increased the slope of the decision front, and made the signal integration unit more sensitive to the activating nutrient signal (Fig 5C). When we analyzed the steady state induction level of the pathway, we found that these network motifs not only altered the sensitivity to the input signals, but also changed the robustness of the response when intracellular protein levels were allowed to fluctuate (see Methods and Models for details).

Discussion

Carbon catabolite repression is a conserved phenomenon across microorganisms, and it has long been established that the yeast GAL pathway is induced when the external glucose concentration drops. Recent studies have shown that yeast cells respond not to a simple glucose threshold, as previously believed, but to the ratio of the external concentrations of galactose and glucose[12]. Our research aimed to determine which molecular circuits could be responsible for ratiometric sensing of nutrient signals. We found that two segments of the sugar uptake/response pathway each had features that could give rise to a ratiometric response. The first of these is the family of transporters that take up the two sugars. Nutrient transporters are not generally considered to be part of signaling pathways or responsible for signal processing, but we found that competition between sugars for transporter binding could explain the ratio-sensing response. The relative binding affinity of the competing carbon sources for the communal transporter determined the concentration ratio for the induction of the GAL pathway. If the two sugars are each allowed to show cooperativity in binding to the transporter, the relative degree of cooperativity determined which sugar the pathway responded to more sensitively. When the cooperativity of galactose binding was overwhelmingly greater than that of glucose binding, the pathway behaved as a galactose threshold sensor; conversely, when the cooperativity of glucose binding was much greater than that of galactose, the pathway only responded to variations in glucose concentration.

The second segment of the sugar uptake/response pathway that can give a ratiometric response is the regulation of transcription. This molecular circuit consists of two sequential reactions, the binding of the intracellular nutrients to their internal sensors, producing an activator complex and a repressor complex, and the binding of these activator/repressor complexes to the cis-regulatory element (CRE) of the GAL1 gene. In this circuit many factors are important for the induction ratio: the relative binding strength between the competing sugars and their corresponding intracellular sensors, the total amount of each type of sensor, and the relative binding strength of the activator complex and the repressor complex to the GAL1 CRE. The behavior of this circuit can be further modulated by introducing negative auto-regulation and/or coherent feedforward loop motifs.

Since both of these elements are found together in the GAL control pathway, we examined how they would work when combined. Concatenating the transporter layer and the transcriptional regulatory layer resulted in ratio-sensing behavior with an expanded dynamical range and increased flexibility. This double-layer model can accommodate a wide and physiologically plausible regime for ratio-sensing by adjusting either the transportation capacity of the

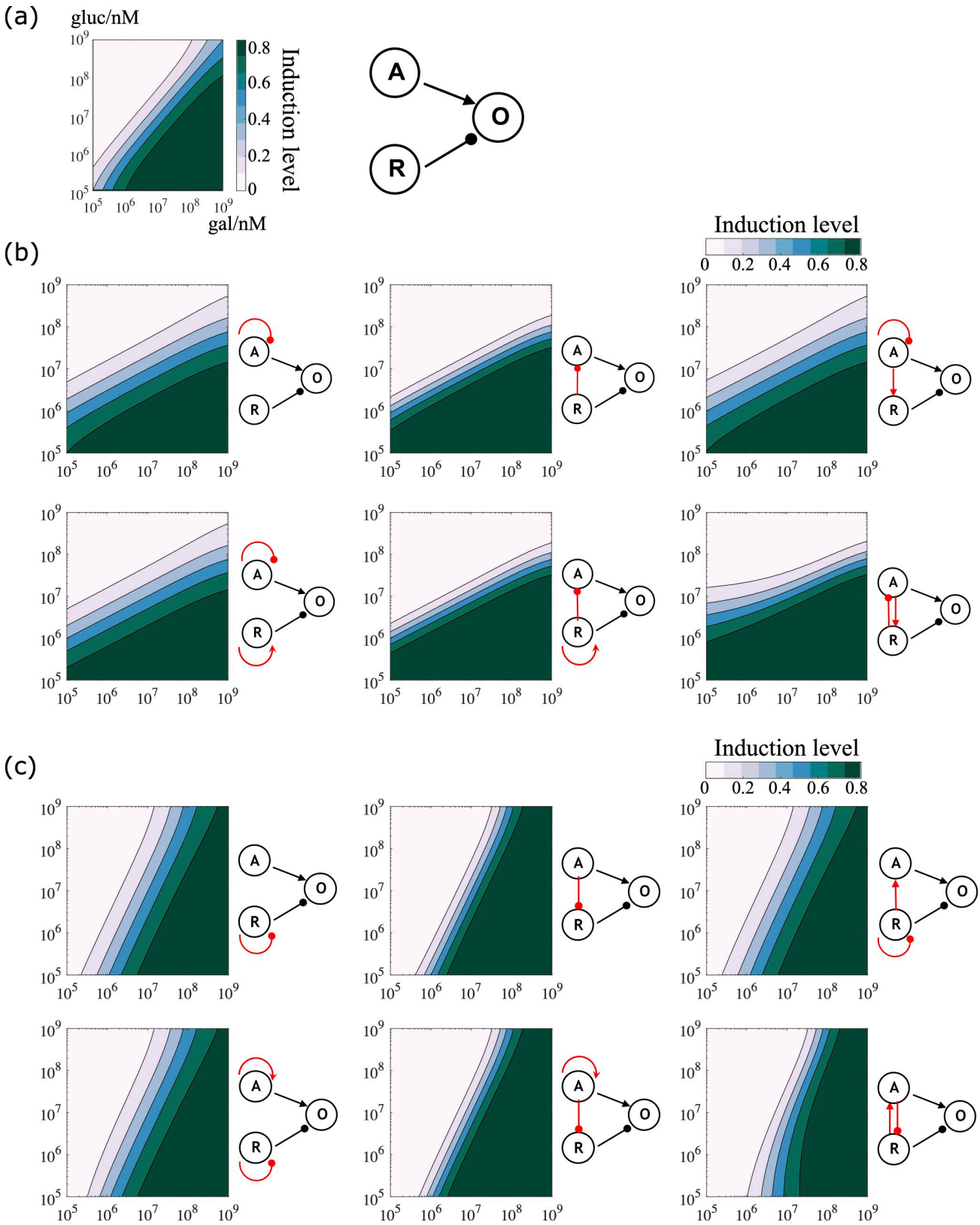

Fig 5. Incorporating network motifs to the basic signal integration unit altered the network sensitivity to input signals. (a) The basic signal integration unit consists of the activator (node A), the repressor (node R), and the output gene (node O). The slope of the decision front for this network is approximately equal to 1. (b) Network topologies that halve the slope of the decision front, i.e. are more susceptible to inhibition by glucose. These topologies involved negative auto-regulation at the activator node and/or an inhibiting edge from the repressor to the activator. (c) Network topologies

that double the slope of the decision front, i.e. are more sensitive to activation by galactose. These topologies involve negative auto-regulation at the repressor node and/or an inhibiting edge from the activator to the repressor. (b)-(c) Parameter values used in these simulations can be found in S5 Table.

https://doi.org/10.1371/journal.pcbi.1007960.g005

transporters or the binding strength between the sugars and their corresponding intracellular sensors. Different strains of yeast that have encountered different conditions during their evolution would therefore be expected to show variation in these parameters.

Our research reveals simple design principles for ratio-sensing signal processing which may be helpful in identifying such behavior in other systems, and can be used to design systems with desirable properties for synthetic biology applications.

Methods and models

The source code for all the simulations and to reproduce all the figures is available at https://github.com/JiayinHong/Computational-study-on-ratio-sensing-in-yeast-galactose-utilization-pathway. A full description and derivations of all the models are provided in the S1 Text.

Modeling competitive binding at transporter level

Sugar transportation can be regarded as a two-step process. First, outside the cellular membrane, extracellular sugars bind to transporters with a forward binding rate kf_{gal}, forming 'loaded' transporters [*gal-T*] or [*gluc-T*], which could dissociate at rate kr_{gal} (though comparatively rather small). Secondly, inside the cellular membrane, the loaded transporters unload sugars into cytoplasm at rate k_{trans}, releasing free transporters and intracellular sugars. Hence, the intracellular sugars are accumulated through transportation of extracellular sugars and balanced by carbon catabolism. We assumed that the total amount of membrane transporters was a constant, and that the transporters could be free, bound by galactose, or bound by glucose. Thus:

$$T_{total} = T_{free} + [gal{-}T] + [gluc{-}T] \tag{10}$$

Using the law of mass action, the levels of intracellular galactose, intracellular glucose, transporters bound by galactose, transporters bound by glucose, and free transporters are related as follows:

$$\frac{dgal_{in}}{dt} = k_{trans} \cdot [gal{-}T] - \gamma \cdot gal_{in} \tag{11}$$

$$\frac{dgluc_{in}}{dt} = k_{trans} \cdot [gluc{-}T] - \gamma \cdot gluc_{in} \tag{12}$$

$$\frac{d[gal{-}T]}{dt} = kf_{gal} \cdot gal_{ex} \cdot T_{free} - kr_{gal} \cdot [gal{-}T] - k_{trans} \cdot [gal{-}T] \tag{13}$$

$$\frac{d[gluc{-}T]}{dt} = kf_{gluc} \cdot gluc_{ex} \cdot T_{free} - kr_{gluc} \cdot [gluc{-}T] - k_{trans} \cdot [gluc{-}T] \tag{14}$$

$$\begin{aligned}\frac{dT_{free}}{dt} = {} & k_{trans} \cdot [gal{-}T] + k_{trans} \cdot [gluc{-}T] + kr_{gal} \cdot [gal{-}T] + kr_{gluc} \cdot [gluc{-}T] \\ & - kf_{gal} \cdot gal_{ex} \cdot T_{free} - kf_{gluc} \cdot gluc_{ex} \cdot T_{free}\end{aligned} \tag{15}$$

When the above reactions reach steady state, the left sides of Eqs (11) to (15) are all equal to 0, and we can derive the levels of these species at steady state. Specifically, we can obtain the intracellular galactose level at steady state as follow:

$$gal_{in} = \frac{k_{trans}}{\gamma} \cdot T_{total} \cdot \frac{1}{1 + \frac{K_{gal}}{gal_{ex}} \cdot \left(1 + \frac{gluc_{ex}}{K_{gluc}}\right)} \tag{16}$$

where $K_{gal} = \frac{kr_{gal} + k_{trans}}{kf_{gal}}$ and $K_{gluc} = \frac{kr_{gluc} + k_{trans}}{kf_{gluc}}$. In a minimal and general transporter regulatory model, we circumvented transcriptional regulatory circuit consisting of Gal3p, Gal80p, and Gal4p. Instead, we proposed a simple yet reasonable assumption for induction of the GAL pathway, which linearly depends on intracellular galactose level. Thus, the contour lines of identical intracellular galactose levels correspond to different induction levels of the pathway in Fig 2.

To derive the expression of the contour lines and solve for the slope and the intercept on *gal* titration axis, we set the fraction in Eq (1) equal to a constant (*const*):

$$\frac{1}{1 + \frac{K_{gal}}{gal_{ex}} \cdot \left(1 + \frac{gluc_{ex}}{K_{gluc}}\right)} = const \tag{17}$$

For instance, when the *const* equals to 0.5, it means that the intracellular galactose level reaches half maximum, corresponding to a half-maximum decision front of the GAL pathway induction.

When $gluc_{ex} \gg K_{gluc}$, Eq (17) in log-log scale is approximately:

$$log\ gluc_{ex} = log\ gal_{ex} + log\frac{K_{gluc}}{K_{gal}} + const' \tag{18}$$

where $const' = \log\left(\frac{1}{const} - 1\right)$. A generalized form of Eq (18) incorporating cooperativity was shown in Eq (2).

Modeling competitive inhibition at transcriptional level

We assumed that GAL1 gene copies within a cell are constant, and that the cis-regulatory element (CRE) of GAL1 could be bound by the activator, bound by the repressor, or free. So, we have,

$$\mathrm{GAL1_{total}} = \mathrm{GAL1_{free}} + \mathrm{GAL1_{active}} + \mathrm{GAL1_{repressed}} \tag{19}$$

The association and dissociation between the sugars and the sensors are as follows:

$$\frac{d\ Activator^*}{dt} = kf_G \cdot gal_{in} \cdot (Activator_{total} - Activator^*) - kr_G \cdot Activator^* \tag{20}$$

$$\frac{d\ Repressor^*}{dt} = kf_M \cdot gluc_{in} \cdot (Repressor_{total} - Repressor^*) - kr_M \cdot Repressor^* \tag{21}$$

The mass actions between the activator, the repressor, and the CRE are as follows:

$$\frac{\mathrm{d\ GAL1_{active}}}{\mathrm{dt}} = \mathrm{kf_A} \cdot \mathrm{GAL1_{free}} \cdot \mathrm{Activator^*} - \mathrm{kr_A} \cdot \mathrm{GAL1_{active}} \tag{22}$$

$$\frac{\mathrm{d\ GAL1_{repressed}}}{\mathrm{dt}} = \mathrm{kf_R} \cdot \mathrm{GAL1_{free}} \cdot \mathrm{Repressor^*} - \mathrm{kr_R} \cdot \mathrm{GAL1_{repressed}} \tag{23}$$

If all the GAL1 gene copies are bound by the activator and thus transcriptionally activated, then the pathway is in its maximum induction. We approximated the induction levels by calculating the actively transcribed GAL1 gene fraction. When the association and dissociation between regulatory factors and CRE reach equilibrium, we could obtain the actively transcribed GAL1 gene fraction as follow

$$\frac{GAL1_{active}}{GAL1_{total}} = \frac{1}{1 + \frac{K_A}{Activator_{total}} \cdot \left(1 + \frac{K_G}{gal_{in}}\right) \cdot \left(1 + \frac{Repressor_{total}}{K_R \cdot \left(1 + \frac{K_M}{gluc_{in}}\right)}\right)} \tag{24}$$

which is equivalent to Eq (5), where $\emptyset_A = \frac{Activator_{total}}{K_A}$, and $\emptyset_R = \frac{Repressor_{total}}{K_R}$.

To obtain the formula for decision front in the transcriptional level model, i.e. Eq (6), we followed similar procedures as that in the transporter model. We set Eq (5) equal to a constant (*const*):

$$\frac{1}{1 + \frac{1}{\emptyset_A} \cdot \left(\frac{K_G}{gal_{in}} + 1\right) \cdot \left(1 + \frac{\emptyset_R}{\frac{K_M}{gluc_{in}} + 1}\right)} = const \tag{25}$$

Again, when the *const* equals to 0.5, it means that half of all the GAL1 gene copies are actively transcribed, corresponding to a half-maximum decision front of the GAL pathway induction.

When $gal_{in} \ll K_G$, $\frac{K_M}{\emptyset_R} \ll gluc_{in} \ll K_M$, Eq (24) is approximately:

$$\frac{1}{1 + \frac{1}{\emptyset_A} \cdot \frac{K_G}{gal_{in}} \cdot \frac{\emptyset_R}{K_M} \cdot gluc_{in}} = const \tag{26}$$

which in log-log scale is:

$$log\ gluc_{in} = log\ gal_{in} + log\frac{K_M}{K_G} + log\frac{\emptyset_A}{\emptyset_R} + const\prime \tag{27}$$

where $const' = \log\left(\frac{1}{const} - 1\right)$.

Introducing network motifs to transcriptional level model

The generalized expression for the actively transcribed fraction of given gene copies is,

$$\mathrm{frac}_{\mathrm{active}} = \frac{1}{1 + \frac{K_A}{A_{total}} \cdot \left(\frac{K_G}{S_A} + 1\right) \cdot \left(1 + \frac{R_{total}}{K_R} \cdot \frac{S_R}{K_M + S_R}\right)} \tag{28}$$

where S_A and S_R represent the concentration of activating input signal and of repressing input signal, respectively. In the case of GAL pathway induction, S_A corresponds to galactose and S_R corresponds to glucose. We studied how different network topologies would alter the actively transcribed fraction of the gene copies, and derived formulas for the decision fronts in various cases. The formulas for the decision fronts are shown and discussed here, while the derivations of equations can be found in S1 Text.

i. Negative auto-regulation at the activator node

We first considered introducing negative auto-regulation to the activator node, which means that making more activators would lead to inhibition of activator expression. We

derived the formula for the decision front in this case as follows:

$$\log S_R = \frac{1}{2}\log S_A + \log\left(\frac{K_M}{\sqrt{K_G}} \cdot \frac{K_R}{K_A} \cdot \frac{\sqrt{A_0 \cdot K_x}}{R_{total}}\right) + \text{const} \quad (29)$$

Eq (28) indicates that incorporating negative auto-regulation at the activator node would halve the slope of the decision front in log-log scale, in other words, the network would become more sensitive to the inhibiting glucose signal. The intercept on the galactose titration axis also becomes dependent on the square root of K_G and A_0, which means that the decision to induce the network is more robust to variation of the binding affinity between galactose and the activator, as well as more robust to the fluctuation of the activator level.

ii. Positive auto-regulation at the activator node

Next, we considered the introduction of positive auto-regulation to the activator node. We found that the formula for the decision front in this case is given by

$$\log S_R = \log\left(S_A - \frac{K_x \cdot K_G}{A_0}\right) + \log\left(\frac{K_M}{K_G} \cdot \frac{K_R}{K_A} \cdot \frac{A_0}{R_{total}}\right) + \text{const} \quad (30)$$

Eq (30) suggests that incorporating positive auto-regulation to the activator changes neither the slope of the decision front, nor the sensitivity to input signals.

iii. Negative auto-regulation at the repressor node

When negative auto-regulation of the repressor is introduced, the formula for the decision front is

$$\log S_R = 2\log S_A + \log\left(\frac{K_M}{K_G^2} \cdot \frac{K_R^2}{K_A^2} \cdot \frac{A_{total}^2}{R_0 \cdot K_y}\right) + \text{const} \quad (31)$$

Eq (31) implies that incorporating negative auto-regulation at the repressor node doubles the slope of the decision front, which means that the network becomes more sensitive to the activating galactose signal. Meanwhile, the intercept on the galactose titration axis becomes dependent on the square of K_G, K_R, K_A and A_{total}, so that the decision to induce the network is more susceptible to variations in the binding affinity between galactose and the activator, or the binding affinity between the regulator and the cis-regulatory element of GAL1, as well as more sensitive to fluctuations in the activator level.

iv. Positive auto-regulation at the repressor node

Similar to the activator node, introducing positive auto-regulation to the repressor node does not change the slope of the decision front. The formula for the decision front is given by:

$$\log\left(S_R - \frac{K_y \cdot K_M}{R_0}\right) = \log S_A + \log\left(\frac{K_M}{K_G} \cdot \frac{K_R}{K_A} \cdot \frac{A_{total}}{R_0}\right) + \text{const} \quad (32)$$

v. Type I incoherent feedforward loop (the activator promotes the repressor)

We next sought to understand how feedforward loops change the integration of the different signals. First, consider the case where the activator promotes the expression of the repressor, forming a type I incoherent feedforward loop (IFFL type I). Solving the formula for the

decision front, we got:

$$\log S_R = \log\left(S_A + \frac{K_y \cdot K_G}{A_{total}}\right) + \log\left(\frac{K_M}{K_G} \cdot \frac{K_R}{K_A} \cdot \frac{A_{total}}{R_0}\right) + \text{const} \quad (33)$$

We found that introducing IFFL type I did not change the network sensitivity to input signals.

vi. Type I coherent feedforward loop (the activator inhibits the repressor)

We next considered the case where the activator inhibited the expression of the repressor, forming type I coherent feedforward loop (CFFL type I). We derived the formula for the decision front:

$$log\ S_R = 2\ log\ S_A + log\left(\frac{K_M}{K_G^2} \cdot \frac{K_R}{K_A} \cdot \frac{A_{total}^2}{R_0 \cdot K_y}\right) + const \quad (34)$$

Eq (34) indicates that incorporating CFFL type I doubles the slope of the decision front in log-log scale, in other words, the network becomes more sensitive to the activating galactose signal. Meanwhile, the intercept on the galactose titration axis becomes dependent on the square of K_G and A_{total}, which means the decision to induce the network is more susceptible to variations in the binding affinity between galactose and the activator, as well as more sensitive to fluctuations in the activator level.

vii. Type II incoherent feedforward loop (the repressor promotes the activator)

We then introduced an activating edge from the repressor to the activator, forming a type II incoherent feedforward loop (IFFL type II). The formula of the decision front in this case is given by:

$$log\left(S_R + \frac{K_x \cdot K_M}{R_{total}}\right) = log\ S_A + log\left(\frac{K_M}{K_G} \cdot \frac{K_R}{K_A} \cdot \frac{A_0}{R_{total}}\right) + const \quad (35)$$

Eq (35) indicates that incorporating IFFL type II does not change the network sensitivity to input signals.

viii. Type II coherent feedforward loop (the repressor inhibits the activator)

Finally, we introduced an inhibitory edge from the repressor to the activator, forming a type II coherent feedforward loop (CFFL type II). The formula of the decision front in this case is given by:

$$log\ S_R = \frac{1}{2} log\ S_A + log\left(\frac{K_M}{\sqrt{K_G}} \cdot \sqrt{\frac{K_R}{K_A}} \cdot \frac{\sqrt{A_0 \cdot K_x}}{R_{total}}\right) + const \quad (36)$$

Eq (36) implies that incorporating CFFL type II halves the slope of the decision front in log-log scale, in other words, the network is more sensitive to the inhibiting glucose signal. The intercept on the galactose titration axis is dependent on the square roots of K_G, K_R, K_A and A_0, which means that the decision to induce the network is more robust to variations in the binding affinity between galactose and the activator, and between the regulators and the cis-regulatory element, as well as more robust to the fluctuation of the activator level.

We further combined auto-regulation with feedforward loops, and studied how they affected network sensitivity to input signals. For either the activator or the repressor, there could be five regulatory states in total: positive auto-regulation, negative auto-regulation,

coherent feedforward loop, incoherent feedforward loop, and without any regulation. As the regulatory states between the activator and the repressor were independent, there were twenty-five possible configurations for the downstream gene expression output. Among them, we found that six configurations that halved the slope of the decision front, i.e. made the system more sensitive to inhibiting glucose signals. These six configurations involved negative auto-regulation of the activator, and/or inhibitory edges from the repressor to the activator. Similarly, there were six configurations that doubled the slope of the decision front, i.e. made the system more sensitive to activating galactose signals. These six configurations involved negative auto-regulation of the repressor, and/or inhibitory edges from the activator to the repressor.

Supporting information

S1 Text. Model derivations and descriptions.
(DOCX)

S1 Table. Parameter descriptions and units.
(DOCX)

S2 Table. Parameter values used in simulations for Fig 2B and 2C.
(DOCX)

S3 Table. Parameter values used in simulations for Fig 3B–3E.
(DOCX)

S4 Table. Parameter values used in simulations for Fig 4C.
(DOCX)

S5 Table. Parameter values used in simulations for Fig 5.
(DOCX)

Acknowledgments

We thank Xiaojing Yang and Yihan Lin for helpful discussions and comments, and Becky Ward for critically reading the manuscript.

Author Contributions

Conceptualization: Jiayin Hong, Bo Hua, Michael Springer, Chao Tang.

Formal analysis: Jiayin Hong.

Funding acquisition: Jiayin Hong, Michael Springer, Chao Tang.

Investigation: Jiayin Hong.

Supervision: Michael Springer, Chao Tang.

Validation: Jiayin Hong, Bo Hua.

Visualization: Jiayin Hong.

Writing – original draft: Jiayin Hong.

Writing – review & editing: Jiayin Hong, Michael Springer, Chao Tang.

References

1. Görke B, Stülke J. Carbon catabolite repression in bacteria: many ways to make the most out of nutrients. Nat Rev Microbiol. 2008 Aug; 6(8):613–24. https://doi.org/10.1038/nrmicro1932 PMID: 18628769
2. Magasanik B. Catabolite Repression. Cold Spring Harb Symp Quant Biol. 1961 Jan 1; 26:249–56. https://doi.org/10.1101/sqb.1961.026.01.031 PMID: 14468226
3. Stülke J, Hillen W. Carbon catabolite repression in bacteria. Curr Opin Microbiol. 1999 Apr; 2(2):195–201. https://doi.org/10.1016/S1369-5274(99)80034-4 PMID: 10322165
4. Kotrba P, Inui M, Yukawa H. Bacterial phosphotransferase system (PTS) in carbohydrate uptake and control of carbon metabolism. Journal of Bioscience and Bioengineering. 2001 Jan 1; 92(6):502–17. https://doi.org/10.1263/jbb.92.502 PMID: 16233138
5. Deutscher J. The mechanisms of carbon catabolite repression in bacteria. Curr Opin Microbiol. 2008 Apr; 11(2):87–93. https://doi.org/10.1016/j.mib.2008.02.007 PMID: 18359269
6. Brückner R, Titgemeyer F. Carbon catabolite repression in bacteria: choice of the carbon source and autoregulatory limitation of sugar utilization. FEMS Microbiol Lett. 2002 Apr; 209(2):141–8. https://doi.org/10.1111/j.1574-6968.2002.tb11123.x PMID: 12007797
7. Monod J. The growth of bacterial cultures. Annual review of microbiology. 1949 Oct; 3(1):371–94.
8. Gancedo JM. Yeast carbon catabolite repression. Microbiology and molecular biology reviews. 1998 Jun 1; 62(2):334–61. PMID: 9618445
9. Johnston M, Flick JS, Pexton T. Multiple mechanisms provide rapid and stringent glucose repression of GAL gene expression in Saccharomyces cerevisiae. Mol Cell Biol. 1994 Jun 1; 14(6):3834–41. https://doi.org/10.1128/mcb.14.6.3834 PMID: 8196626
10. Lohr D, Venkov P, Zlatanova J. Transcriptional regulation in the yeast GAL gene family: a complex genetic network. FASEB J. 1995 Jun 1; 9(9):777–87. https://doi.org/10.1096/fasebj.9.9.7601342 PMID: 7601342
11. Wang J, Atolia E, Hua B, Savir Y, Escalante-Chong R, Springer M. Natural variation in preparation for nutrient depletion reveals a cost–benefit tradeoff. PLoS Biol. 2015 Jan 27; 13(1):e1002041. https://doi.org/10.1371/journal.pbio.1002041 PMID: 25626068
12. Escalante-Chong R, Savir Y, Carroll SM, Ingraham JB, Wang J, Marx CJ, et al. Galactose metabolic genes in yeast respond to a ratio of galactose and glucose. Proc Natl Acad Sci. 2015 Feb 3; 112 (5):1636–41. https://doi.org/10.1073/pnas.1418058112 PMID: 25605920
13. Wang X, Xia K, Yang X, Tang C. Growth strategy of microbes on mixed carbon sources. Nature communications. 2019 Mar 20; 10(1):1–7. https://doi.org/10.1038/s41467-018-07882-8 PMID: 30602773
14. Antebi YE, Linton JM, Klumpe H, Bintu B, Gong M, Su C, et al. Combinatorial Signal Perception in the BMP Pathway. Cell. 2017 Sep 7; 170(6):1184–1196.e24. https://doi.org/10.1016/j.cell.2017.08.015 PMID: 28886385
15. Boles E, Hollenberg CP. The molecular genetics of hexose transport in yeasts. FEMS Microbiol Rev. 1997 Aug; 21(1):85–111. https://doi.org/10.1111/j.1574-6976.1997.tb00346.x PMID: 9299703
16. Özcan S, Johnston M. Function and Regulation of Yeast Hexose Transporters. Microbiol Mol Biol Rev. 1999 Sep 1; 63(3):554–69. PMID: 10477308
17. Maier A, Völker B, Boles E, Fuhrmann GF. Characterisation of glucose transport in *Saccharomyces cerevisiae* with plasma membrane vesicles (countertransport) and intact cells (initial uptake) with single Hxt1, Hxt2, Hxt3, Hxt4, Hxt6, Hxt7 or Gal2 transporters. FEMS Yeast Res. 2002 Dec; 2(4):539–50. https://doi.org/10.1111/j.1567-1364.2002.tb00121.x PMID: 12702270
18. Jordan P, Choe J-Y, Boles E, Oreb M. Hxt13, Hxt15, Hxt16 and Hxt17 from *Saccharomyces cerevisiae* represent a novel type of polyol transporters. Sci Rep. 2016 Mar 21; 6:23502. https://doi.org/10.1038/srep23502 PMID: 26996892
19. Tschopp JF, Emr SD, Field C, Schekman R. GAL2 codes for a membrane-bound subunit of the galactose permease in Saccharomyces cerevisiae. J Bacteriol. 1986 Apr; 166(1):313–8. https://doi.org/10.1128/jb.166.1.313-318.1986 PMID: 3082856
20. Bhat PJ, Hopper JE. Overproduction of the GAL1 or GAL3 protein causes galactose-independent activation of the GAL4 protein: evidence for a new model of induction for the yeast GAL/MEL regulon. Molecular and cellular biology. 1992 Jun 1; 12(6):2701–7. https://doi.org/10.1128/mcb.12.6.2701 PMID: 1317007
21. Bhat PJ, Murthy TVS. Transcriptional control of the GAL/MEL regulon of yeast Saccharomyces cerevisiae: mechanism of galactose-mediated signal transduction. Mol Microbiol. 2001 Jun; 40(5):1059–66. https://doi.org/10.1046/j.1365-2958.2001.02421.x PMID: 11401712
22. Giniger E, Varnum SM, Ptashne M. Specific DNA binding of GAL4, a positive regulatory protein of yeast. Cell. 1985 Apr 1; 40(4):767–74. https://doi.org/10.1016/0092-8674(85)90336-8 PMID: 3886158

23. Platt A, Reece RJ. The yeast galactose genetic switch is mediated by the formation of a Gal4p-Gal80p-Gal3p complex. EMBO J. 1998 Jul 15; 17(14):4086–91. https://doi.org/10.1093/emboj/17.14.4086 PMID: 9670023

24. Torchia TE, Hamilton RW, Cano CL, Hopper JE. Disruption of regulatory gene GAL80 in Saccharomyces cerevisiae: effects on carbon-controlled regulation of the galactose/melibiose pathway genes. Mol Cell Biol. 1984 Aug; 4(8):1521–7. https://doi.org/10.1128/mcb.4.8.1521 PMID: 6092916

25. Timson DJ, Ross HC, Reece RJ. Gal3p and Gal1p interact with the transcriptional repressor Gal80p to form a complex of 1:1 stoichiometry. Biochem J. 2002 May 1; 363(Pt 3):515–20. https://doi.org/10.1042/0264-6021:3630515 PMID: 11964151

26. Torchia TE, Hopper JE. Genetic and molecular analysis of the GAL3 gene in the expression of the galactose/melibiose regulon of Saccharomyces cerevisiae. Genetics. 1986 Jun 1; 113(2):229–46. PMID: 3013721

27. Lutfiyya LL, Iyer VR, DeRisi J, DeVit MJ, Brown PO, Johnston M. Characterization of Three Related Glucose Repressors and Genes They Regulate in Saccharomyces cerevisiae. Genetics. 1998 Dec 1; 150(4):1377–91. PMID: 9832517

28. Carlson M. Glucose repression in yeast. Curr Opin Microbiol. 1999 Apr 1; 2(2):202–7. https://doi.org/10.1016/S1369-5274(99)80035-6 PMID: 10322167

29. Schüller H-J. Transcriptional control of nonfermentative metabolism in the yeast Saccharomyces cerevisiae. Curr Genet. 2003 Jun; 43(3):139–60. https://doi.org/10.1007/s00294-003-0381-8 PMID: 12715202

30. Santangelo GM. Glucose signaling in Saccharomyces cerevisiae. Microbiology and Molecular Biology Reviews. 2006 Mar 1; 70(1):253–82. https://doi.org/10.1128/MMBR.70.1.253-282.2006 PMID: 16524925

31. Bennett MR, Pang WL, Ostroff NA, Baumgartner BL, Nayak S, Tsimring LS, et al. Metabolic gene regulation in a dynamically changing environment. Nature. 2008 Aug 28; 454(7208):1119–22. https://doi.org/10.1038/nature07211 PMID: 18668041

32. Gunawardena J. A linear framework for time-scale separation in nonlinear biochemical systems. PloS one. 2012 May 14; 7(5):e36321. https://doi.org/10.1371/journal.pone.0036321 PMID: 22606254

33. Milo R, Shen-Orr S, Itzkovitz S, Kashtan N, Chklovskii D, Alon U. Network Motifs: Simple Building Blocks of Complex Networks. Science. 2002 Oct 25; 298(5594):824–7. https://doi.org/10.1126/science.298.5594.824 PMID: 12399590

34. Alon U. Network motifs: theory and experimental approaches. Nat Rev Genet. 2007 Jun; 8(6):450–61. https://doi.org/10.1038/nrg2102 PMID: 17510665

35. Tyson JJ, Novák B. Functional Motifs in Biochemical Reaction Networks. Annu Rev Phys Chem. 2010 Mar; 61(1):219–40. https://doi.org/10.1146/annurev.physchem.012809.103457 PMID: 20055671

36. Madar D, Dekel E, Bren A, Alon U. Negative auto-regulation increases the input dynamic-range of the arabinose system of Escherichia coli. BMC Syst Biol. 2011 Jul 12; 5(1):111. https://doi.org/10.1186/1752-0509-5-111 PMID: 21749723

37. Rosenfeld N, Elowitz MB, Alon U. Negative Autoregulation Speeds the Response Times of Transcription Networks. J Mol Biol. 2002 Nov 8; 323(5):785–93. https://doi.org/10.1016/s0022-2836(02)00994-4 PMID: 12417193

38. Mangan S, Alon U. Structure and function of the feed-forward loop network motif. Proc Natl Acad Sci. 2003 Oct 14; 100(21):11980–5. https://doi.org/10.1073/pnas.2133841100 PMID: 14530388